Theoretical Chemistry Accounts (2019) 138:51
https://doi.org/10.1007/s00214-019-2442-1

REGULAR ARTICLE

Structural, bonding, and superhalogen properties of $Au_4X_4^{-/0}$ (X = F, Cl, Br, and I) clusters

Sheng-Jie Lu[1] · **Li-Shun Wu**[1] · **Feng Lin**[1]

Received: 11 February 2019 / Accepted: 28 March 2019 / Published online: 6 April 2019

Abstract

The structural, bonding, and superhalogen properties of $Au_4X_4^{-/0}$ (X = F, Cl, Br, and I) clusters were investigated by density functional theory calculations. Our results found that $Au_4F_4^-$, $Au_4Cl_4^-$, and $Au_4Br_4^-$ have similar cyclic arrangements, spectral, and superhalogen features, and $Au_4I_4^-$ has a D_{4h} symmetric planar ring-like structure, while Au_4X_4 neutrals all adopt a D_{2d} symmetric quasi-planar eight-membered ring. Bond lengths, Wiberg bond orders, molecular orbital, ELF, and PDOS analyses suggest that the Au–I and Au–Au bonding in $Au_4X_4^{-/0}$ are weak involving both covalent and ionic contributions. The nucleus-independent chemical shift, aromatic stabilization energy, and multicenter bond index calculations suggest that $Au_4I_4^-$ has significant aromaticity.

Keywords Gold halides · Superhalogen · Aromaticity

1 Introduction

Gold halides have attracted considerable attention because they are extensively applied in catalysts and solid materials [1, 2]. It has been demonstrated that the relativistic effects of Au atom can facilitate 6*s*–5*d* hybridization [3]; as a result, the diverse oxidation states are available for Au atom. Also, the Au–Au bond in gold clusters frequently displays intriguing properties, such as the extremely bonding distances and aurophilic interactions [3], and Au atom exhibits similar bonding properties with hydrogen in its interaction with the other atoms [4, 5]. Due to the remarkably large electronegativity and high electron affinity of gold, it can act as a good electron acceptor [6].

Halides are also usually considered as an electron acceptor. However, the gold-containing compounds show significant covalent bonding characters and unique structural arrangements [7]. Then, one can raise the questions that what are the structural and bonding properties in gold halides? To answer these questions, there are a lot of investigations focused on exploring the geometrical characteristics and electronic properties of gold halides [8–17]. AuF_6^- can be named as superhalogen as the result of its electron affinity (EA) being to be 10 ± 0.5 eV [18], and can also be used as superhalogen anion to form $LiAuF_6$ ionic salt [19–21]. The Au atom exhibits + 7 oxidation states in AuF_7 [22], which can be synthesized by reacting AuF_5 with atomic fluorine [23]. A combined study of $[XAuCN]^-$ (X = F − I) based on anion photoelectron spectroscopy and theoretical calculations revealed that the Au–F bond has strong ionic characters and the covalent bonding strength gradually increases from Au–Cl to Au–I [24, 25]. Very recently, the first-principles calculations of coinage fluorides under high pressure identified that the Au atoms in AuF_4 and AuF_6 stable molecular crystals have oxidation states of + 4 and + 6, respectively [26].

Nevertheless, the previous investigations regarding the structures and properties of gold halides mainly focused on the monomeric gold halides, whereas those of multiple gold halides are rare [27–29]. In addition, the bonding nature (ionic or covalent) of multiple gold halides is still controversial. It is interesting to study multiple gold halides because these clusters may hold very special geometrical structures

Electronic supplementary material The online version of this article (https://doi.org/10.1007/s00214-019-2442-1) contains supplementary material, which is available to authorized users.

✉ Sheng-Jie Lu
lushengjie@iccas.ac.cn

✉ Li-Shun Wu
wu-lishun@163.com

[1] Department of Chemistry and Chemical Engineering, Heze University, Heze 274015, Shandong Province, China

and exhibit unique fascinating properties. More importantly, investigating the multiple gold halides may provide valuable information for the production of functional nanomaterials for solar cell or lithium battery. Here, we explored the structural, bonding, and superhalogen properties of isolated $Au_4X_4^{-/0}$ (X = F, Cl, Br, and I) clusters using density functional theory calculations. We found that $Au_4F_4^-$, $Au_4Cl_4^-$, and $Au_4Br_4^-$ have similar cyclic structures and superhalogen features, and $Au_4I_4^-$ possesses a D_{4h} symmetric aromatic planar structure, whereas Au_4X_4 neutrals adopt D_{2d} symmetric quasi-planar eight-membered ring structures.

2 Theoretical methods

Density functional theory (DFT) within B3LYP framework [30, 31] was performed for the configuration optimizations and frequency calculations of both anionic and neutral Au_4X_4 (X = F, Cl, Br, and I) clusters. Previously, the B3LYP functional was also used in investigating the structures and properties of gold halides [27–29]. The aug-cc-pVTZ-PP basis sets [32, 33] were chosen for the Au and I atoms, whereas the aug-cc-pVTZ basis sets [34, 35] were applied for the F, Cl, and Br atoms. No symmetry constraint was used in the configuration optimizations and frequency calculations. The CALYPSO software [36] was applied for an unbiased search for initial structures of $Au_4X_4^{-/0}$ clusters. Details of obtaining the initial structures based on the CALYPSO software have been elaborated elsewhere [37–40]. Also, the structures of the neutral gold fluoride and chloride clusters reported in the previous works [27–29] had been considered in the structural optimization processes. To determine the lowest energy spin states of $Au_4X_4^{-/0}$ clusters, the 2, 4, and 6 spin states were taken into account for anionic clusters. As for neutral Au_4X_4 clusters, the 1, 3, and 5 spin states were considered. Harmonic vibrational frequency calculations were performed to verify that the obtained structures are the true minima. As for both anionic and neutral Au_4X_4 clusters, no imaginary frequencies were found to confirm the low-lying isomers are the genuine minima on their potential energy surfaces. The TPSSH functional [41] and B3PW91 functional [31] were also used in the configuration optimizations and frequency calculations. The TPSSH functional gives generally excellent results for a wide range of systems and properties, correcting overestimated bond lengths in molecules including clusters, hydrogen-bonded complexes, and ionic solids [41]. The B3PW91 functional performs significantly better than previous functionals with gradient corrections only and fits experimental atomization energies with an impressively small average absolute deviation of 2.4 kcal/mol [31]. Also, in the previous investigations of clusters including Au atoms [42, 43], B3PW91 functional is widely applied to explore their structures and properties. Therefore, in this work, we used TPSSH and B3PW91 functionals to conduct the compared calculations with B3LYP functional. We calculated the theoretical vertical detachment energies (VDEs) by the energy differences of the neutrals and anions both using the anionic geometries, while we obtained the theoretical adiabatic detachment energies (ADEs) through the energy differences of the neutrals and anions using their each global minimum. During calculating the relative energies and ADEs of isomers, we performed zero-point energy (ZPE) corrections. The atomic dipole moment corrected Hirshfeld population (ADCH) analyses, implanted in the Multiwfn program [44], were conducted to probe the atomic charge distributions of $Au_4X_4^{-/0}$ clusters. Compared with Mulliken, natural population analysis (NPA), and atoms in molecules (AIM) charges, the ADCH charge has many advantages in handling with atomic charge distribution, such as the ADCH atomic charges are very reasonable in chemical sense, molecular dipole moment is exactly reproduced, the reproducibility of electrostatic potential (ESP) is close to the atomic charges from fitting ESP, and the computational cost of ADCH correction is almost zero [45, 46]. Theoretical calculations were performed within the Gaussian 09 [47].

3 Theoretical results and discussion

The low-lying isomers of $Au_4X_4^-$ anions are displayed in Fig. 1. Also, the relative energies (ΔE) and theoretical VDEs and ADEs of isomers are shown in Fig. 1. As we all known, anion photoelectron spectroscopy has been extensively used for studying atomic or molecular clusters because it can obtain the fingerprint information of both anionic and neutral species. However, the experimental photoelectron spectra of $Au_4X_4^-$ anions have not been reported. In this work, the photoelectron spectra of the lowest-lying isomers of $Au_4X_4^-$ anions were simulated based on the generalized Koopmans' theorem (GKT) [48, 49], as displayed in Fig. 2. We hope that these theoretical results can help the experimentalists to understand the further experimental spectra. As for Au_4X_4 neutrals, their low-lying isomers as well as ΔE are presented in Fig. 3.

3.1 $Au_4F_4^-$/Au_4F_4

One can see from Fig. 1 that the lowest-lying isomer (A) of $Au_4F_4^-$ is a cyclic structure, in which the four F atoms attach to the different sites of Au-capped Au_3 triangle framework. The Au–F bond lengths are in the range of 1.94–2.29 Å, whereas the Au–Au bond lengths are between 2.57 and 2.77 Å. The bond angles of Au–Au–Au and Au–F–Au are 118.9° and 79.9°, respectively. Isomer A is also the lowest-lying isomer for $Au_4F_4^-$ at the TPSSH and B3PW91 levels. The VDE (5.67 eV) and ADE (5.26 eV) of isomer A are

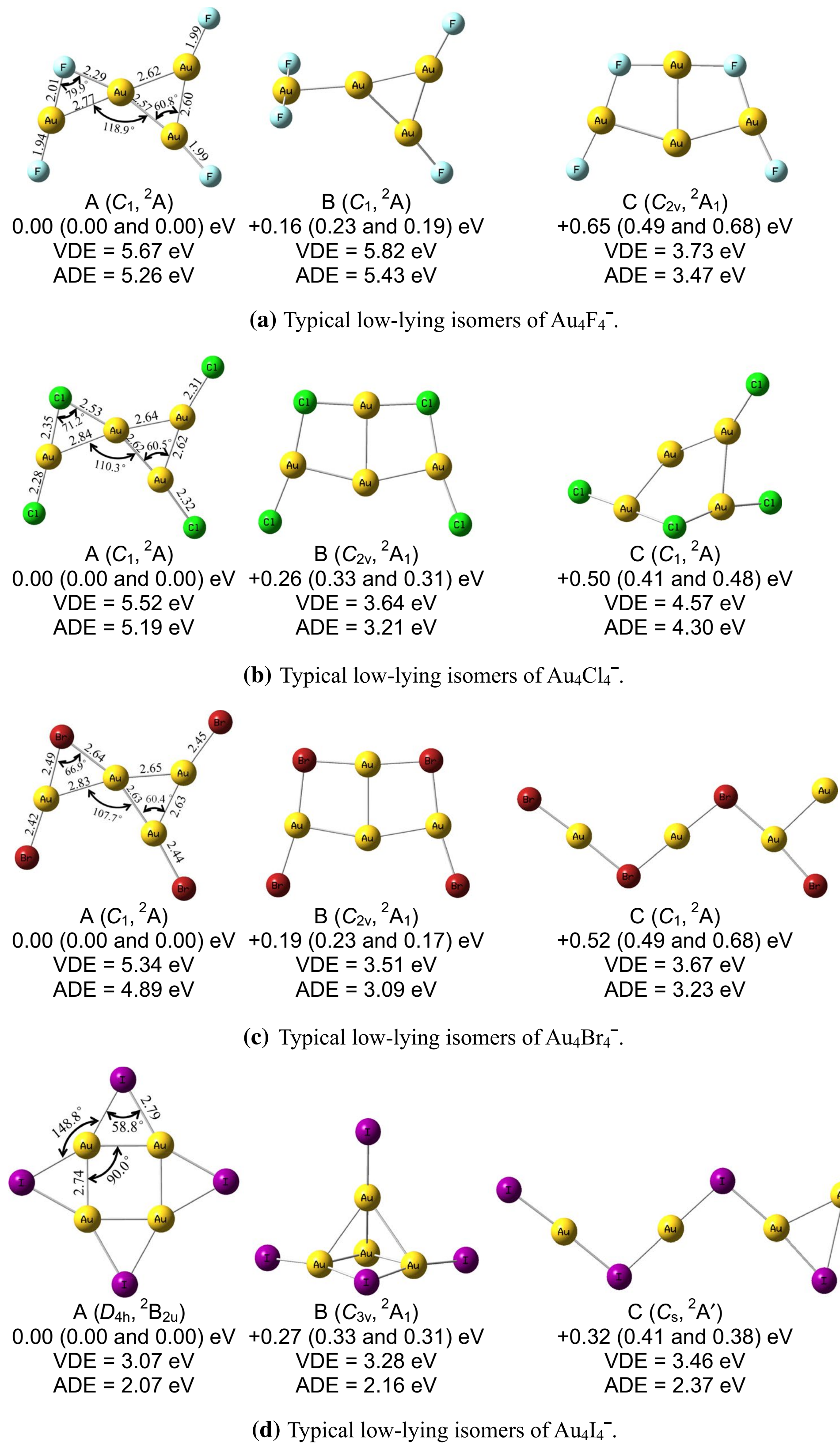

Fig. 1 Typical low-lying isomers of $Au_4X_4^-$ (X = F, Cl, Br, and I) as well as their relative energies, ADEs, and VDEs obtained at the B3LYP level. The relative energies in parentheses are calculated at the TPSSH and B3PW91 levels. The bond lengths of the lowest-lying isomers of $Au_4X_4^-$ are given in angstrom

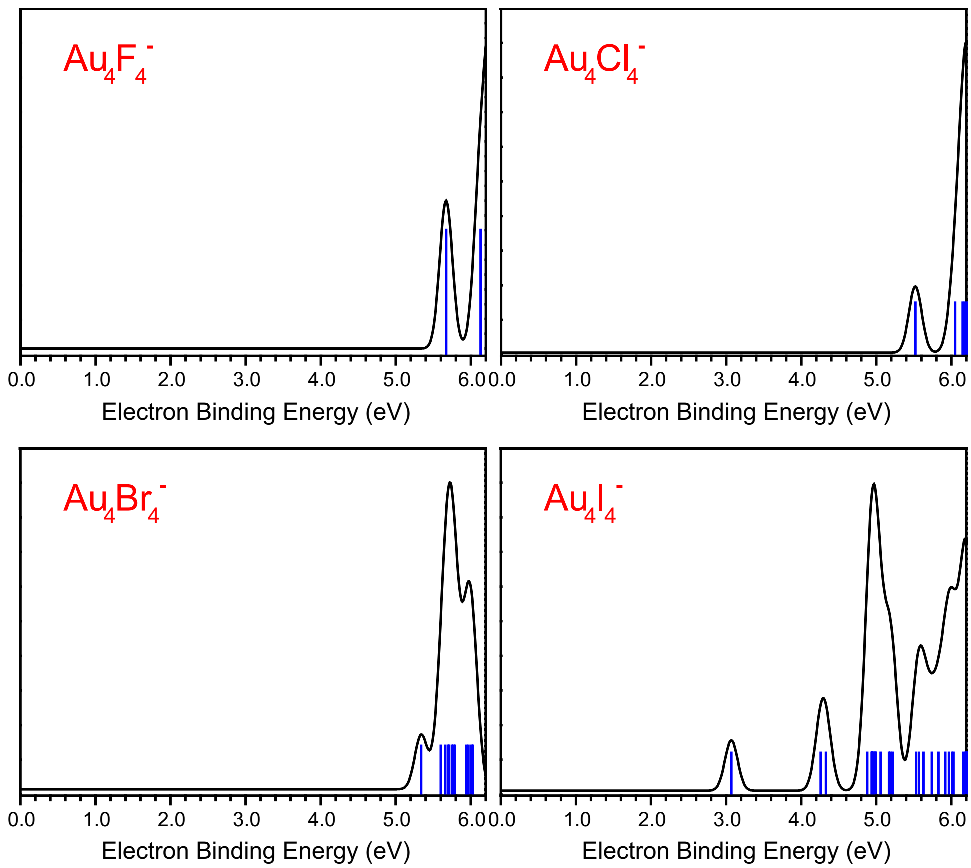

Fig. 2 Simulated photoelectron spectra of the lowest-lying isomers of $Au_4X_4^-$ (X = F, Cl, Br, and I). Simulated spectrum was obtained by fitting the distribution of the transition lines with the unit area Gaussian functions of 0.20 eV full widths at half maximum. The vertical lines in blue are the calculated vertical detachment energies for $Au_4X_4^-$ (X = F, Cl, Br, and I)

significantly larger than the EA of Cl (3.61 eV) [50]; as a result, $Au_4F_4^-$ can be classified as a superhalogen anion to form a $LiAu_4F_4$ ionic salt. We can see from Fig. 2 that the simulated photoelectron spectrum of isomer A has a relatively weak peak at 5.67 eV and a high-intensity peak at 6.17 eV. Isomers B and C are located above the lowest-lying isomer by 0.16 and 0.65 eV, respectively, calculated at the B3LYP level. The calculated relative energies are slightly different at the different theoretical levels.

The lowest-lying isomer (A′) of Au_4F_4 is a D_{2d} symmetric quasi-planar ring-like structure in which the four F atoms edge-cap the four Au–Au bonds of Au_4 square core, different from its corresponding anionic counterpart. The Au–F and Au–Au bond lengths are 2.07 and 3.04 Å, respectively. The bond angles of Au–Au–Au, Au–F–Au, and F–Au–F are 90.0°, 94.9°, and 175.1°, respectively. The other isomers are higher in energy than the lowest-lying isomer by at least 0.21 eV at the B3LYP level.

3.2 $Au_4Cl_4^-$/Au_4Cl_4

The most stable isomer (A) of $Au_4Cl_4^-$ is very similar to that of $Au_4F_4^-$ anion. The Au–Cl bond lengths are in the range of 2.28–2.53 Å, whereas the Au–Au bond lengths are between 2.62 and 2.84 Å. The bond angles of Au–Au–Au and Au–Cl–Au are 110.3° and 71.2°, respectively. Also, isomer A is the most stable isomer for $Au_4Cl_4^-$ at the TPSSH and B3PW91 levels. The VDE and ADE of isomer A are 5.52 and 5.19 eV, respectively, much larger than the EA of its Cl (3.61 eV) [50] building block; thus, $Au_4Cl_4^-$ can be considered as a superhalogen anion to form a $LiAu_4Cl_4$ ionic salt. It is reasonable to find that the simulated photoelectron spectra of $Au_4Cl_4^-$ and $Au_4F_4^-$ have similar spectral features due to their analogical structural characteristics. The other isomers are higher in energy than the lowest-lying isomer by at least 0.26 eV at the B3LYP level. The calculated relative energies among the three isomers are slightly different at the TPSSH and B3PW91 levels.

As we can see from Fig. 3, the most stable isomer of Au_4Cl_4 neutral (A′) is a D_{2d} symmetric quasi-planar ring-like structure composed of four Cl–Au–Cl chain-shaped units sharing with four Cl atoms. The bonding Au–Cl distance is 2.34 Å, and the bond angles of Au–Cl–Au and Cl–Au–Cl are 89.5° and 177.8°, respectively. The dihedral angle between two Au–Cl–Au–Cl planes is 12.8°. The other isomers are higher in energy than the lowest-lying isomer by at least 0.65 eV at the B3LYP level.

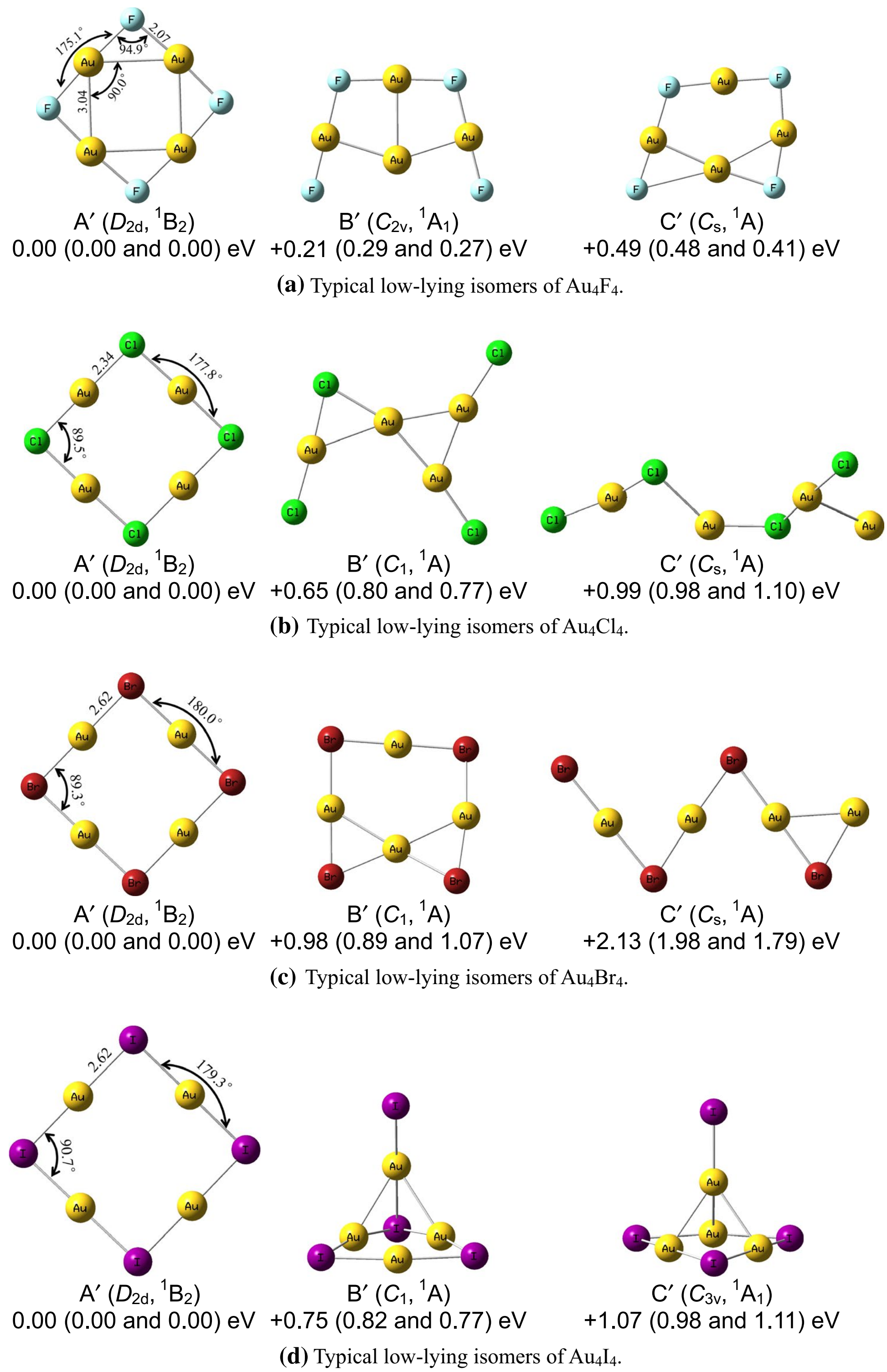

Fig. 3 Typical low-lying isomers of Au_4X_4 (X = F, Cl, Br, and I) as well as their relative energies obtained at the B3LYP level. The relative energies in parentheses are calculated at the TPSSH and B3PW91 levels. The bond lengths of the lowest-lying isomers of Au_4X_4 are given in angstrom

(a) Typical low-lying isomers of Au_4F_4.

(b) Typical low-lying isomers of Au_4Cl_4.

(c) Typical low-lying isomers of Au_4Br_4.

(d) Typical low-lying isomers of Au_4I_4.

3.3 $Au_4Br_4^-/Au_4Br_4$

The global minimum (isomer A) of $Au_4Br_4^-$ resembles well with those of $Au_4F_4^-$ and $Au_4Cl_4^-$. The Au–Br bond lengths are between 2.42 and 2.49 Å, and the Au–Au bond lengths are within the scope of 2.63–2.83 Å. The bond angles of Au–Au–Au and Au–Br–Au are calculated to be 107.7° and 66.9°, respectively. Likewise, isomer A is the most stable one for $Au_4Br_4^-$ at the TPSSH and B3PW91 levels. Additionally, the VDE and ADE of isomer A are calculated to be 5.34 and 4.89 eV, respectively; they both far exceed the EA of Cl (3.61 eV) [50]; as a consequence, $Au_4Br_4^-$ is also a superhalogen anion. Given that $Au_4Br_4^-$, $Au_4Cl_4^-$, and $Au_4F_4^-$ adopt very similar geometrical structures, it is very reasonable to find their analogical photoelectron spectral patterns, as we can see from Fig. 2. The other isomers are higher in energy than the global minimum by at least 0.19 eV at the B3LYP level.

Likewise, the global minimum (A′) of Au_4Br_4 adopts a D_{2d} symmetric quasi-planar ring-like structure. The bonding Au–Br distance is 2.62 Å, and the bond angles of Au–Br–Au and Br–Au–Br are 89.3° and 180.0°, respectively. The dihedral angle between two Au–Br–Au–Br planes is 7.2°. The other isomers are higher in energy than the global minimum by at least 0.98 eV at the B3LYP level. Isomer A′ is also the most stable isomer for Au_4Cl_4 at TPSSH and B3PW91 levels.

3.4 $Au_4I_4^-$/Au_4I_4

The isomer A of $Au_4I_4^-$ is a D_{4h} symmetric planar structure, in which the four I atoms edge-cap the four Au–Au bonds of Au_4 square core. The Au–I and Au–Au bond lengths are 2.79 and 2.74 Å, respectively. The bond angles of Au–Au–Au, Au–I–Au, and I–Au–I are 90.0°, 58.8°, and 148.8°, respectively. The VDE and ADE of isomer A are computed to be 3.07 and 2.07 eV, respectively. In the simulated photoelectron spectrum of isomer A, it reveals three peaks at 3.07, 4.30, and 5.05 eV, and several congested peaks at the high electron binding energy (EBE) region. The spectral features of $Au_4I_4^-$ are markedly different from those of $Au_4F_4^-$, $Au_4Cl_4^-$, and $Au_4Br_4^-$. The two peaks in the simulated spectrum have a large space of 1.23 eV, more likely due to the highly symmetric structure of $Au_4I_4^-$. The other isomers are higher in energy than isomer A by at least 0.27 eV at the B3LYP level. Isomer A is also the most stable one for $Au_4I_4^-$ at the TPSSH and B3PW91 levels, and the calculated relative energies of isomers are slightly different.

The global minimum (A′) of Au_4I_4 is a D_{2d} symmetric quasi-planar eight-membered ring structure, composed of four I–Au–I chain-shaped units sharing with four I atoms. The global minimum of Au_4I_4 neutral (A′) resembles well with those of Au_4F_4, Au_4Cl_4, and Au_4Br_4. The bonding Au–I distance is 2.62 Å, and the bond angles of Au–I–Au and I–Au–I are 90.7° and 179.3°, respectively. The dihedral angle between two Au–I–Au–I planes is calculated to be only 1.5°. The other two isomers are higher in energy than isomer A by at least 0.75 eV at the B3LYP level.

Here, we would like to point out that the calculated VDEs of $Au_4X_4^-$ decrease gradually from 5.67 to 3.07 eV with the variation from X = F to I. This is probably because of the different interactions between halogen and gold atoms due to the various properties of halogen atoms including the atomic radiuses, electronegativities, and electron affinities. In particular, the covalent interactions between Au and I atoms are weakest among these mixed clusters because the covalent bonding lengths gradually increase from Au–F to Au–I, as shown in Fig. 1. Certainly, the highly symmetric geometric structure of $Au_4I_4^-$ may be another reason for the lower VDE. As for $Au_4X_4^-$, the Au–Au distances increase gradually from X = F to Br, suggesting that the Au–Au interactions are weaken. Moreover, the global minima of Au_4X_4 neutrals are consistent with the results in previous investigations [27–29].

On the one hand, we found that $Au_4F_4^-$, $Au_4Cl_4^-$, and $Au_4Br_4^-$ have similar geometrical structures, spectral features, and superhalogen property, which are significantly different from $Au_4I_4^-$. As for their corresponding neutral counterparts, they all adopt analogical quasi-planar eight-membered ring structures. On the other hand, among these Au–X mixed clusters, the four Au atoms incline to interact with each other and form an Au–Au bond, while the four halogen atoms prefer to bonding with the Au atoms rather than interact with each other. These suggest that the structures and properties of Au–X mixed clusters are not completely similar. In particular, $Au_4I_4^-$ has a D_{4h} symmetric planar structure. The different structural evolutions between $Au_4X_4^-$ (X = F, Cl, and Br) and $Au_4I_4^-$ clusters may be due to the involved 5*p* orbitals of I atoms interacted with the 5*d* orbitals of Au atoms (see subsequent molecular orbital analyses). In particular, it is well recognized that the relativistic effect of I atom can promote *s*–*p* hybridization, giving rise to the I atom having a wide range of oxidation states from − 1 to + 7 in chemical reactions [6], even though iodine is not as reactive as its group elements F_2, Cl_2, and Br_2. These unique properties and effects of I may lead to the structural evolution and bonding properties of Au–I mixed clusters are different from those of Au–X (X = F, Cl, and Br) clusters. The Au–I bond lengths in $Au_4I_4^-$ are calculated to be 2.79 Å, much longer than that (2.47 Å) in the AuI diatomic molecule [51], suggesting that the Au–I bonds are weak, in good agreement with the low calculated Wiberg bond orders of Au–I bonds (0.50). The weak covalent Au–I and Au–Au bonds in $Au_4I_4^-$ can be further confirmed by molecular orbital analyses.

The molecular orbitals of the lowest-lying isomer of $Au_4I_4^-$ are shown in Fig. 4. The SOMO is primarily made up of the $5d_{x^2-y^2}$ and 6*s* orbitals of Au and the $5p_x$ and $5p_y$ orbitals of I. The HOMO-1, HOMO-2, HOMO-3, HOMO-4, and HOMO-5 are mainly composed of 5*d* orbitals of Au atoms and 5*p* orbitals of I atoms. It is worth noting that there are small overlaps between 5*d* orbitals of Au atoms and 5*p* orbitals of I atoms. Also, the small mixings between the 5*d* orbitals of four Au atoms are found. These can confirm that the covalent Au–I and Au–Au bonds are weak. The weaker Au–I and Au–Au interactions in $Au_4I_4^-$, in comparison with those in $Au_4F_4^-$, $Au_4Cl_4^-$, and $Au_4Br_4^-$, which may partly explain why the calculated VDE of $Au_4I_4^-$ is

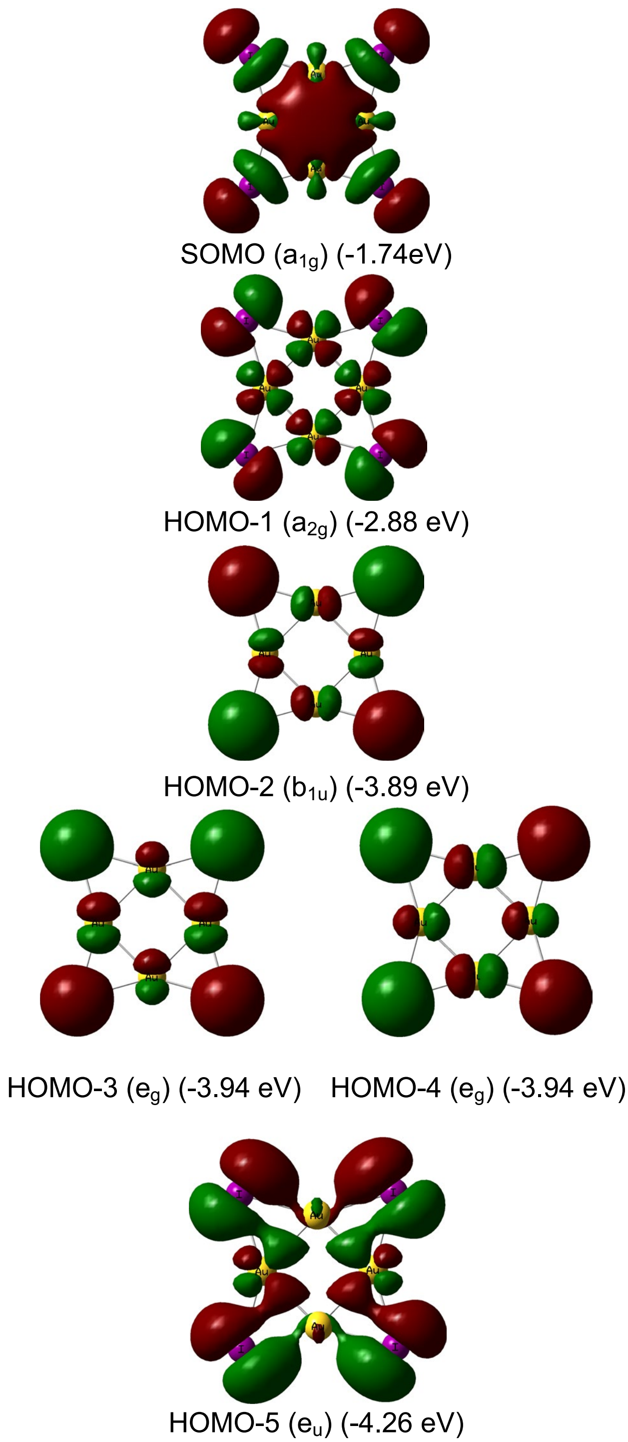

Fig. 4 Molecular orbitals of the lowest-lying isomer of $Au_4I_4^-$ (D_{4h}, $^2B_{2u}$, isosurface value = 0.02) at the B3LYP level

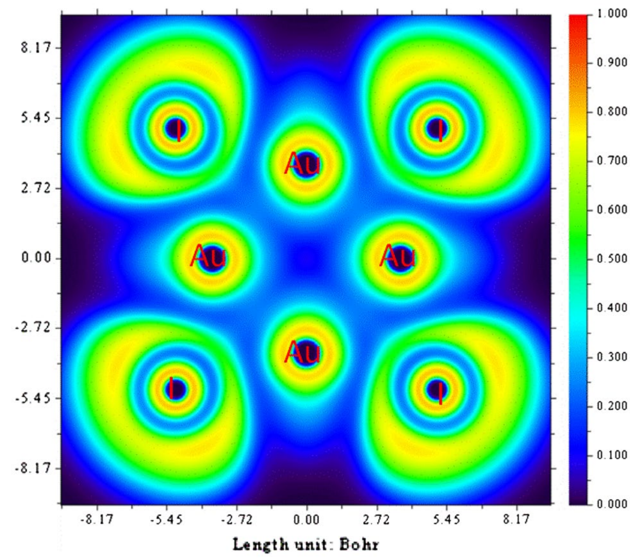

Fig. 5 Electron localization functions analysis of $Au_4I_4^-$

the lowest one (the calculated Wiberg bond orders of Au–X bonds (0.55–0.79) and Au–Au bonds (0.40–0.58) in $Au_4F_4^-$, $Au_4Cl_4^-$, and $Au_4Br_4^-$).

The electron localization function (ELF) analyses of $Au_4I_4^-$ are shown in Fig. 5. ELF was initially proposed by Becke and Edgecombe [52] and is used to measure the probability of electron pairing. In general, the larger ELF value means more strong the covalent bond. We can clearly see from Fig. 5 that the ELF values of Au–I and Au–Au bonds are within the scope of 0.2–0.3, indicating that the covalent Au–I and Au–Au bonds are weak. This is in accordance with the analysis results of bond lengths, calculated Wiberg bond orders, and molecular orbitals. A direct calculation of bond dissociation energies of $Au_4I_4^-$ anion was also carried out to reinforce the statement of a weak covalent bonding for Au–I and Au–Au bonds, which suggests that the dissociation energies of Au–I and Au–Au bonds are averagely calculated to be 26.9 and 19 kcal/mol, respectively.

The Au–I and Au–Au interactions can also be interpreted based on the partial density of states (PDOS), as presented in Fig. 6. As for the four Au atoms, it exhibits very small overlaps between Au_4-*d* and Au_4-*s*, confirming that the four Au atoms have weak aurophilic interactions. Regarding the Au–I interactions, there are small overlaps between Au_4-*d* and I_4-*p* states at − 2.0 to − 6.0 eV, indicating the Au–I interactions are also weak. Also, these suggest that the bonding interactions are in the order of Au–I > Au–Au. It seems that the Au–I interactions can weaken the Au–Au interactions of Au_4 framework. The PDOS analyses are consistent with the molecular orbital and ELF analyses. Therefore, the weak covalent Au–I and Au–Au interactions play crucial role in thermal stabilities of $Au_4I_4^-$, similar to the weak interactions in proteins [53].

To probe the effective atomic charge distributions in $Au_4I_4^-$, the ADCH analyses were carried out. The ADCH charges on the four Au atoms and four I atoms are + 0.11*e* and − 0.36*e*, respectively, suggesting that there are electrons

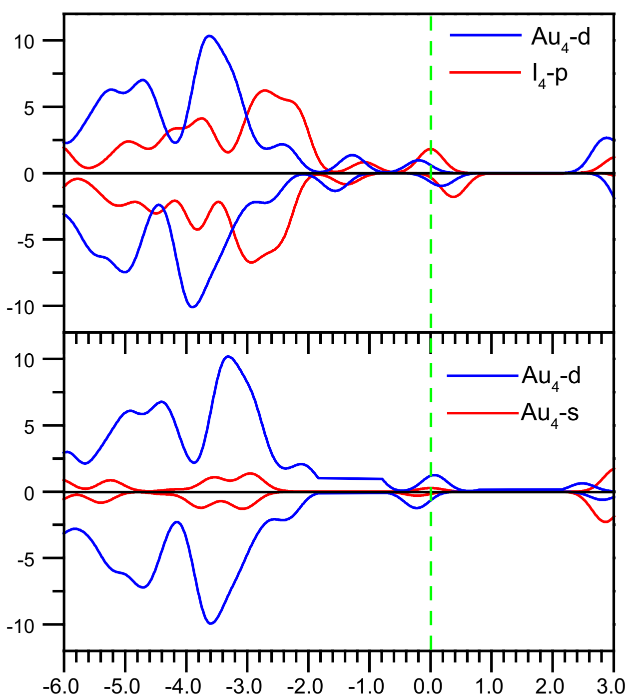

Fig. 6 Partial density of states (PDOS) of $Au_4I_4^-$. Green dashed line is the Fermi level

transferring from the Au_4 framework to these I atoms. The electron transfer can be probably explained by the stronger electronegativity of I atom ($\chi = 2.66$) than Au atom ($\chi = 2.54$) [54]. The electron transfer may play crucial role in stabilizing the planar structure of $Au_4I_4^-$. Thus, except for the covalent character, the Au–I bonds also exhibit some ionic characters due to the transfer of 6*s* electrons from Au atoms to the 5*p* orbitals of I atoms. Overall, based on the molecular orbitals, ELF, calculated Wiberg bond orders, PDOS, and ADCH analyses, we can conclude that the D_{4h} symmetric planar structure is stabilized by both covalent and ionic bonds.

Aromaticity stemming from electron delocalization is also used for comprehending the stability of $Au_4I_4^-$. The nucleus-independent chemical shift (NICS) value of $Au_4I_4^-$ is computed at the B3LYP/aug-cc-pVTZ-PP level. The calculated results suggested that $Au_4I_4^-$ has a large NICS value of −46.5 ppm; therefore, $Au_4I_4^-$ exhibits significant aromaticity. The aromatic stabilization energy (ASE) [55] and multicenter bond index [56] at the B3LYP/aug-cc-pVTZ-PP level can further identify the aromaticity of $Au_4I_4^-$. The aromatic stabilization energy (ASE) is based on energy to analyze the aromaticity due to electron delocalization. The system is aromatic when the reaction energy is positive. Generally, the system is regarded to be aromatic when the ASE > 5 kcal/mol. Here, the ASE of $Au_4I_4^-$ is calculated as the equation of $\mathrm{ASE}(Au_4I_4^-) = 2E(Au_2I_3^-) - 2E(I) - E(Au_4I_4^-) = 14.6$ kcal/mol (the E is the total energy including zero-point energy (ZPE) corrections). The higher multicenter bond index refers to be the stronger aromaticity. The calculations of multicenter bond index for $Au_4I_4^-$ were carried out using Multiwfn program [44], and the multicenter bond index of $Au_4I_4^-$ is calculated to be 0.97. Most noteworthy, the typical aromatic compounds in organic chemistry such as benzene, where the HOMO exhibit mainly z-character. Here, the SOMO is mainly contributed by the $5d_{x^2-y^2}$ and 6*s* orbitals of Au atoms. The aromaticity may be come from the spherically symmetric 6*s* orbitals of Au atoms.

Here, the structures of $Au_4I_4^{-/0}$ are compared with those of $Cu_4I_4^{-/0}$ reported in our previous work [37]. $Au_4I_4^-$ is a D_{4h} symmetric planar structure, slightly different from that of $Cu_4I_4^-$, which is a C_{2h} symmetric planar structure, in which the four I atoms surround with the Cu_4 rhomb. As for neutrals, Au_4I_4 adopts a D_{2d} symmetric quasi-planar eight-membered ring structure, while that of Cu_4I_4 neutral holds a D_{2d} symmetric V-shaped structure. These suggest that the geometrical configurations of Cu and Au–I hybrid clusters are different, although the Cu and Au atoms are in the same group.

We also carried out an unbiased search for initial structures of Cu–X and Ag–X (X = F, Cl, Br, and I) hybrid clusters using CALYPSO software and optimized their geometrical structures at the B3LYP level, and the results are displayed in Figs. S1, S2, S3, and S4 (see them in Supplementary Materials). Here, it is interesting to compare the structures of Cu–X, Ag–X, and Au–X (X = F, Cl, Br, and I) hybrid clusters. As for anions, the global minima of $TM_4X_4^-$ (TM = Cu, Ag, and Au; X = F, Cl, Br, and I) all have a similar planar structure with the four X atoms surrounding the TM_4 rhombic framework with slightly different symmetries. As for neutrals, the most stable isomers of TM_4X_4 (TM = Cu, Ag, and Au; X = F, Cl, Br, and I) adopt a quasi-planar eight-membered ring-like structure except for Ag_4F_4 and Cu_4I_4. Ag_4F_4 is a planar structure with the four F atoms surrounding the Ag_4 rhombic framework, similar to its corresponding anion, and Cu_4I_4 adopts D_{2d} symmetric V-shaped structure.

4 Conclusions

We carried out a DFT theoretical study of structural, bonding, and superhalogen properties of $Au_4X_4^{-/0}$ (X = F, Cl, Br, and I) clusters. We found that $Au_4F_4^-$, $Au_4Cl_4^-$, and $Au_4Br_4^-$ anions have similar cyclic structures, spectral features, and superhalogen property, while $Au_4I_4^-$ anion adopts a D_{4h} symmetric planar structure. Au_4X_4 (X = F, Cl, Br, and I) neutrals all has a D_{2d} symmetric quasi-planar eight-membered ring structure. The Au–I and Au–Au bonds in $Au_4I_4^-$ are weak including the covalent and ionic characters.

The weak covalent Au–I and Au–Au interactions can be further verified by the bond lengths, Wiberg bond orders molecular orbital, ELF, and PDOS. The large NICS value of −46.5 ppm, aromatic stabilization energy (ASE), and multicenter bond index indicate that $Au_4I_4^-$ is significantly aromatic.

5 Supplementary materials

Cartesian coordinates for the low-lying isomers of $Au_4X_4^{-/0}$, and typical low-lying isomers of $Cu_4X_4^-$ and $Ag_4X_4^-$ (X = F, Cl, Br, and I) obtained at the B3LYP level.

Acknowledgements This work was supported by the Natural Science Foundation of Shandong Province, China (Grant No. ZR2018BB040), Open Funds of Beijing National Laboratory for Molecular Sciences (Grant No. BNLMS201804), and research start-up funds (Doctoral Science Foundation, Grant No. XY18BS02) of Heze University.

References

1. Lu X, Tuan H-Y, Korgel BA, Xia Y (2008) Chem Eur J 14:1584
2. Kang SK, Yoon SK, Kim Y (2001) Org Lett 3:2697
3. Pyykkö P (2004) Angew Chem Int Ed 43:4412
4. Li Q, Li H, Li R, Jing B, Liu Z, Li W, Luan F, Cheng J, Gong B, Sun J (2011) J Phys Chem A 115:2853
5. Kiran B, Li X, Zhai HJ, Cui LF, Wang LS (2004) Angew Chem Int Ed 43:2125
6. Pyykkö P (1988) Chem Rev 88:563
7. Wang LS (2010) Phys Chem Chem Phys 12:8694
8. Schulz A, Hargittai M (2001) Chem Eur J 7:3657
9. Hargittai M, Schulz A, Reffy B, Kolonits M (2001) J Am Chem Soc 123:1449
10. Koirala P, Willis M, Kiran B, Kandalam AK, Jena P (2010) J Phys Chem C 114:16018
11. Okabayashi T, Yamazaki E, Tsukamoto K, Tanimoto M (2003) J Mol Spectrosc 220:155
12. Craciun R, Picone D, Long RT, Li S, Dixon DA, Peterson KA, Christe KO (2010) Inorg Chem 49:1056
13. Li H, Li Q, Li R, Li W, Cheng J (2011) J Chem Phys 135:074304
14. Li X (2014) J Comput Chem 35:923
15. Evans CJ, Gerry MCL (2000) J Am Chem Soc 122:1560
16. Laerdahl JK, Saue T Jr, Fægri K (1997) Theor Chem Acc 97:177
17. Evans CJ, Gerry MC (2000) J Mol Spectrosc 203:105
18. Compton RN (1978) J Chem Phys 68:2023
19. Graudejus O, Elder SH, Lucier GM, Shen C, Bartlett N (1999) Inorg Chem 38:2503
20. Lucier GM, Shen C, Elder SH (1998) Inorg Chem 37:3829
21. Riedel S, Kaupp MC (2009) Chem Rev 45:10497
22. Riedel S, Kaupp M (2006) Inorg Chem 45:1228
23. Timakov AA, Prusakov VN, Drobyshevskii YV (1986) Dokl Akad Nauk SSSR 21:125
24. Wang YL, Wang XB, Xing XP, Wei F, Li J, Wang LS (2010) J Phys Chem A 114:11244
25. Liu HT, Xiong XG, Dau PD, Wang YL, Li J, Wang LS (2011) Chem Sci 2:2101
26. Lin J, Zhang S, Guan W, Yang G, Ma Y (2018) J Am Chem Soc 140:9545
27. Rabilloud F (2012) J Comput Chem 33:2083
28. Zhou Z-J, Hu Y-F (2012) Z Naturforsch 67a:99
29. Dore EM, Lyon JT (2016) J Clust Sci 27:1365
30. Lee C, Yang W, Parr RG (1988) Phys Rev B Condens Matter Mater Phys 37:785
31. Becke AD (1993) J Chem Phys 98:5648
32. Peterson KA, Shepler BC, Figgen D, Stoll H (2006) J Phys Chem A 110:13877
33. Peterson KA, Puzzarini C (2005) Theor Chem Acc 114:283
34. Dunning TH Jr (1989) J Chem Phys 90:1007
35. Woon DE, Dunning TH Jr (1993) J Chem Phys 98:1358
36. Lv J, Wang YC, Zhu L, Ma YM (2012) J Chem Phys 137:084104
37. Lu S-J, Wu L-S, Lin F (2018) Comput. Theor. Chem. 1139:102
38. Lu S-J, Wu L-S, Lin F (2018) Chem Phys Lett 707:108
39. Lu S-J (2018) Chem Phys Lett 713:58
40. Lu S-J, Xu H-G, Xu X-L, Zheng W-J (2017) J Phys Chem C 121:11851
41. Tao J, Perdew JP, Staroverov VN, Scuseria GE (2003) Phys Rev Lett 91:146401
42. Adamo C, Barone V (1999) J Chem Phys 110:6158
43. Perdew JP, Burke K, Ernzerhof M (1996) Phys Rev Lett 77:3865
44. Lu T, Chen FW (2012) J Comput Chem 33:580
45. Lu T, Chen FW (2012) J Theor Comput Chem 11:163
46. Lu T, Chen FW (2012) Acta Phys Chim Sin 28:1
47. Frisch MJ, Trucks GW, Schlegel HB, Scuseria GE, Robb MA, Cheeseman JR, Scalmani G, Barone V, Mennucci B, Peterson KA, Nakatsuji H, Caricato M, Li X (2009) Gaussian 09, Revision A.02. Gaussian Inc, Wallingford
48. Tozer DJ, Handy NC (1998) J Chem Phys 109:10180
49. Akola J, Manninen M, Häkkinen H, Landman U, Li X, Wang LS (1999) Phys Rev B Condens Matter Mater Phys 60:297
50. Berzinsh U, Gustafsson M, Hanstorp D, Klinkmüller A, Ljungblad U, Mårtensson-Pendrill A-M (1995) Phys Rev A 51:231
51. Reynard LM, Evans CJ, Gerry MCL (2001) J Mol Spectrosc 205:344
52. Becke AD, Edgecombe KE (1990) J Chem Phys 92:5397
53. Ibrahim BS, Pattabhi V (2016) Sci China Chem 59:1270
54. Pauling L (1932) J Am Chem Soc 54:3570
55. Lewars E (2007) Computational chemistry—introduction to the theory and applications of molecular and quantum mechanics, 2nd edn. Kluwer Academic Publishers, New York, p P307
56. Giambiagi M, Giambiagi MSD, Mundim KC (1990) Struct Chem 1:423